

Triangulation candidates for Bayesian optimization

Robert B. Gramacy* Annie Sauer† Nathan Wycoff‡

December 15, 2021

Abstract

Bayesian optimization is a form of sequential design: idealize input-output relationships with a suitably flexible nonlinear regression model; fit to data from an initial experimental campaign; devise and optimize a criterion for selecting the next experimental condition(s) under the fitted model (e.g., via predictive equations) to target outcomes of interest (say minima); repeat after acquiring output under those conditions and updating the fit. In many situations this “inner optimization” over the new-data acquisition criterion is cumbersome because it is non-convex/highly multi-modal, may be non-differentiable, or may otherwise thwart numerical optimizers, especially when inference requires Monte Carlo. In such cases it is not uncommon to replace continuous search with a discrete one over random candidates. Here we propose using candidates based on a Delaunay triangulation of the existing input design. In addition to detailing construction of these “tricands”, based on a simple wrapper around a conventional convex hull library, we promote several advantages based on properties of the geometric criterion involved. We then demonstrate empirically how tricands can lead to better Bayesian optimization performance compared to *both* numerically optimized acquisitions and random candidate-based alternatives on benchmark problems.

Key words: surrogate modeling, Gaussian process, active learning, sequential design, space-filling design, Delaunay triangulation, convex hull

1 Introduction

This paper addresses the classic continuous unconstrained optimization problem

$$x^* = \operatorname{argmin}_{x \in \mathcal{B}} f(x) \tag{1}$$

where the bounding box \mathcal{B} is a hyperrectangle, often taken as $[0, 1]^d$ in coded inputs. The objective $f : \mathcal{B} \rightarrow \mathbb{R}$ is a *blackbox* function, meaning that its operations are generally opaque to us, and we can only learn about its behavior through (expensive) evaluation. Often, f is a numerical simulation carried out on a computer, where expense is measured in core-hours. Such problems are most challenging when f is highly non-convex, and thus contains multiple

*Department of Statistics, Virginia Tech; *authors listed alphabetically*

†Corresponding author: Department of Statistics, Virginia Tech, anniees@vt.edu

‡Massive Data Institute, McCourt School of Public Policy, Georgetown University

local minima. Consequently the tacit goal of a solver is to minimize the number of times that f is evaluated in search of a global solution.

The earliest papers on so-called Bayesian optimization (BO) were developed as a means of adapting statistical modeling and design principles to optimization in the face of high simulation expense (Moćkus, 1975; Jones et al., 1998). Examples of physics-based simulators exhibiting such characteristics are provided by Pourmohamad and Lee (2021); scenarios in machine learning are reviewed by Garnett (2022). BO is common in studies of engagement and user experiences in online platforms (e.g., Letham and Bakshy, 2019), hyperparameter estimation for deep learning (e.g. Turner et al., 2021; Feurer et al., 2018) and materials design (e.g. Zhang et al., 2020b), comprising a non-representative sample of recent examples.

To illustrate the canonical approach to BO, and thereby introduce the main contributions in this paper, consider $f(x) = \sin(x)$ and $\mathcal{B} = [-1, 2\pi + 1]$. Suppose we evaluated f at six equally-spaced inputs x and that we have fit a response surface \hat{f}_n , a so-called surrogate model (Gramacy, 2020), to data (X_n, Y_n) , where $y_i = f(x_i)$, for $i = 1, \dots, n = 6$. The canonical surrogate is a Gaussian process (GP) regression, and this is what we shall use here, but the methodology is agnostic to that choice so long as the predictive equations from \hat{f}_n have similar features – e.g., non-linear and with growing uncertainty away from the training data sites. Therefore, we shall not review GPs and instead use notation $\mu_n(x)$ and $\sigma_n(x)$ to abstract the moments of such a surrogate.

The top-left panel of Figure 1 shows a fitted \hat{f}_6 via μ_6 as solid black line with error bars $\mu_6 \pm 2\sigma_6$ as dashed-red lines. Each of the one-hundred gray lines in the plot is a sample from the predictive distribution. Notice that this distribution interpolates the training data (black dots), a GP hallmark. Although we shall exclusively entertain f 's without noise, this is not a limitation of BO nor our own contributions. Further discussion is tabled until Section 5. The current best run $f_n^{\min} = \min\{y_1, \dots, y_n\}$ is located near $x = 5$, but there is considerable predictive uncertainty about other, untried parts of the input space \mathcal{B} , relative to f_n^{\min} . Just eyeballing it, locations anywhere in $[-1, 0] \cup [4, 6] \cup [2\pi, 2\pi + 1]$ look promising.

The BO literature is filled with so-called *acquisition criteria* which operationalize that casual observation. We shall focus on two and note that several others are variations on similar themes. One is called *Thompson sampling* (TS; Thompson, 1933), and involves sampling from the predictive distribution $Y(x) \sim \hat{f}_n \mid X_n, Y_n$ and choosing $x_{n+1} = \operatorname{argmin}_{x \in \mathcal{B}} Y(x)$. TS amounts to randomly selecting one of those gray lines and optimizing it in lieu of the expensive f , so the criterion is inherently stochastic. The other is called *expected improvement* (EI; Jones et al., 1998). Define *improvement* as $I(x) = \min\{0, f_{\min}^n - Y(x)\}$ and take its expectation with respect to $Y(x) \sim \hat{f}_n \mid X_n, Y_n$. This expectation has a closed form for Gaussian $Y(x) \sim \hat{f}_n$, as furnished by GPs:

$$\begin{aligned} \text{EI}(x) &= \mathbb{E}\{I(X)\} = \int I(x) dY(x) & (2) \\ &= (f_{\min}^n - \mu_n(x)) \Phi\left(\frac{f_{\min}^n - \mu_n(x)}{\sigma_n(x)}\right) + \sigma_n(x) \phi\left(\frac{f_{\min}^n - \mu_n(x)}{\sigma_n(x)}\right). \end{aligned}$$

However, we are not limited to that choice: one can always resort to Monte Carlo expectation instead. The bottom-left panel of Figure 1 provides EI for surrogate \hat{f}_6 . Contrary to TS,

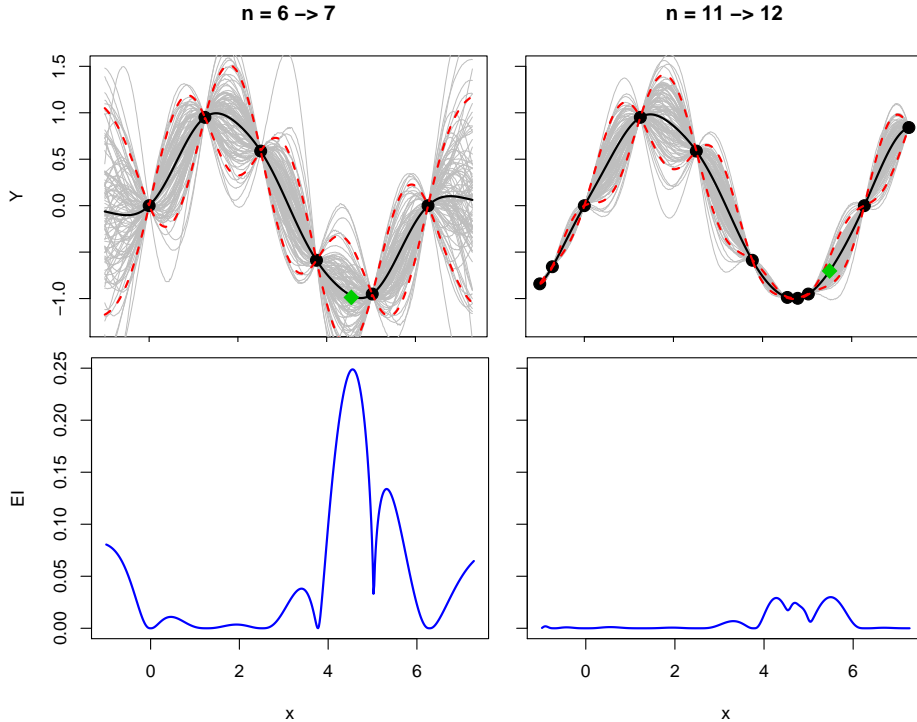


Figure 1: Left column: predictive surface (top) via means (solid black), 90% intervals (dashed-red), and sample paths (gray) after a space-filling design; with EI (bottom) and resulting acquisition (green diamond, $n = 6 \rightarrow 7$). Right column: the same after five EI-based acquisitions ($n = 11 \rightarrow 12$).

the EI acquisition $x_{n+1} = \operatorname{argmax}_{x \in \mathcal{B}} \text{EI}(x)$ can be deterministic, if properly solved. This $n = 7^{\text{th}}$ point is shown as a green diamond on the panel above. The right column of panels in Figure 1 shows the resulting surfaces after five such EI-optimizing acquisitions.

Observe that both TS and EI involve “inner-optimizations” over a criterion, a task that may be even more challenging than the original problem (1). Each gray line is highly multimodal, as is the EI surface. Both have about as many local optima as there are training data points n , whereas the original $f(x)$ has only two minima in \mathcal{B} . Speedy evaluation of $\mu_n(x)$ and $\sigma_n(x)$ relative to expensive $f(x)$ saves us, but only partly. We still need to find good x_{n+1} without exhaustive search or other cumbersome subroutines.

Two strategies are common, sometimes separately, sometimes in tandem as a hybrid. The simplest option is to distribute N candidate points \mathcal{X}_N throughout the input space, evaluate the criterion on \mathcal{X}_N , and thereby replace a continuous search with a discrete one. In low input dimension, like 1d and maybe 2d, you can use a dense grid of candidates effectively. In higher dimension one usually chooses \mathcal{X}_N via limited space-filling design like a random Latin hypercube sample (LHS; McKay et al., 1979) to manage the computational expense of evaluating the criterion exhaustively. A higher-powered approach would be to use a derivative-based numerical local optimization library such as L-BFGS-B (Byrd et al., 2003).

Derivatives may be approximated by finite-differencing or may be available in closed form depending on the criterion and nature of \hat{f}_n . The former requires more computer work and some consideration of numerical stability; the latter more researcher/programmer effort when possible (Monte Carlo-based \hat{f}_n challenges this approach). Pure candidate-based search is most common with TS because of its stochastic nature. Derivative-based continuous search is popular in simple GP/EI setups, but a multi-start scheme is essential to avoid inferior local solutions. This is where the hybrids come in: candidates seeding local solvers.

In this paper we contend that both strategies, random space-filling candidates and multi-start local optimization, can be replaced by more thoughtfully chosen \mathcal{X}_N . In the 1d setting of Figure 1 we could place candidates at the midway point between each of the existing n inputs and the boundary \mathcal{B} , implementing a kind of multi-pronged bisection search (Burden and Faires, 1985, Section 2.1). This would result in $N = n + 1 = 7$ candidates in the left column and $N = n + 1 = 12$ on the right. The best of those \mathcal{X}_N by either criterion might not give a precise solution to the inner optimization, but it would be an accurate one because both EI and any of the random gray lines indicate a solution close to one of those midway points. Both green diamonds are slightly off-center of midway, but the midway value is almost as good, *and* could be much better than one of the inferior local modes that might otherwise be found by a limited random candidate or multi-start local search scheme.

You might argue that this 1d example is contrived and overly simplistic, and we would generally agree. In fact, we shall explicitly target two and higher dimensions going forward. First, in Section 2 we shall scale-up the midway candidate idea to what we call “tricands”, based on Delaunay triangulation and the convex hull of the existing training-data inputs. These may be calculated by library subroutines. We explore tricands’ features and limitations, suggest remedies with the BO application in mind, and detail our open source implementation. In Section 3 we demonstrate that tricands outperform both random LHS candidates and a multi-start derivative-based/BFGS inner optimization for solving the acquisition criterion when surrogate GP predictive equations are available in closed form. In Section 4 we consider two modern, nonstationary surrogates requiring Markov chain Monte Carlo (MCMC) in which closed-form acquisition criteria are not readily available, thwarting local derivative-based inner-optimization. Candidates are essential in this setting, and our tricands are better than random space-filling ones. We conclude with a lengthy discussion in Section 5 covering application outside of BO and other extensions. Perhaps the single greatest selling point for tricands is how easy they are to insert into an existing BO setup by swapping our implementation in place of another candidate-based scheme.

2 Delaunay triangulation candidates

Many criteria for BO resemble Eq. (2), balancing exploitation ($\mu_n(x)$ below f_{\min}^n) with exploration ($\sigma_n(x)$ big). Most nonlinear regression models inflate predictive uncertainty ($\sigma_n(x)$) away from training data locations X_n . In the case of GPs, this is what produces the “sausage shaped” predictive intervals shown as red-dashed lines in Figure 1. The main insight in this paper is that careful allocation of candidates *between* existing training data locations, where

$\sigma_n(x)$ is high, allows for BO acquisitions that do not necessitate cumbersome numerical optimization of posterior predictive quantities but still balance exploitation and exploration. In other words, a hard statistical optimization can be replaced with an easier geometric one.

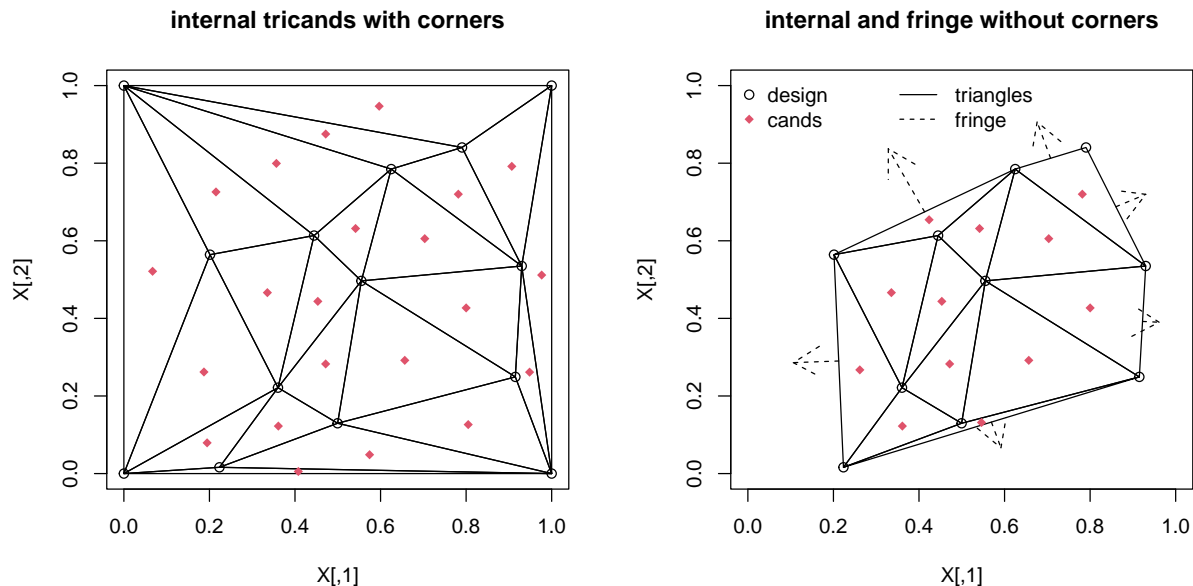


Figure 2: Illustrating interior candidates (left) and interior and fringe ones (right) based on a Delaunay triangulation (solid lines).

The idea is sketched graphically in Figure 2, whose details will emerge over the next two subsections. The existing design X_n is shown as open circles, and the selected candidates are closed red dots *and* the tips of dashed arrows. We call these interior (Section 2.1) and fringe (Section 2.2) candidates, respectively. Both are calculated based on Delaunay triangles and their convex hull, outlined by solid black lines in the figure, explained next. Throughout this section we provide illustrations in 2d to ease visualization; however, our target is higher dimensional input spaces as shall be borne out in our examples in Section 3 and beyond.

2.1 Interior candidates

A *Delaunay triangulation* of X_n is an angle-maximizing set of d line-segments connecting geographically nearby points, such that no point lies inside the circumcircle of those points. Such triangulations subdivide the interior of the *convex hull* of X_n , which is the the smallest (convex) set that contains those points. In 2d, lines depicting those subdivisions form triangles. In higher dimension they form tetrahedra, however one often abuses the nomenclature and still refers to triangles. A more precise definition requires unwinding those of several other geometric criteria, which are easy to track down on Wikipedia, and would be a distraction to this discussion. Delaunay triangulation is the dual of a Voronoi tessellation, which has been deployed for divide-and-conquer-based nonstationary surrogate modeling (e.g., Kim

et al., 2005; Rushdi et al., 2017), imposing both statistical and computational independence. We are unaware of any design or active-learning uses of triangulation.

Figure 2 shows triangulations for two similar X_n . The set on the right is a more common situation, where the coordinates X_n were chosen at random and the convex hull forms a (convex but otherwise non-regular) polygon. On the left the same X_n is augmented with four corner points in $\mathcal{B} = [0, 1]^2$ so that the convex hull is a square, which changes the triangulation on its fringe. Observe that the part of the triangulation concerning the points on the interior, i.e., those which are within the convex hull in the right panel, is unchanged.

There are fast algorithms for calculating Delaunay triangulations, the best of which leverage such nesting for divide-and-conquer. In 2d, these have $\mathcal{O}(n \log n)$ runtimes. In higher dimension such analysis is more complicated due to the number of triangles, which depends on the geometry of X_n , a topic we shall return to shortly. For R we use `geometry` on CRAN (Habel et al., 2019); for Python we use `Delaunay` in `scipy.spatial`. Both are wrappers around a C library called `Qhull` implementing “quickhull” (Barber et al., 1996).

This triangulation provides the framework for our BO candidates. Let the triangles be denoted by T_j , for $j = 1, \dots, n_T$. Allow us to table a discussion of how n_T relates to the design size n . Each T_j is a $(d + 1) \times d$ matrix when X_n has d columns. In 2d this is 3×2 , providing the vertices of a triangle. In higher dimension these are the vertices of a tetrahedron. Create n_T new candidates \mathcal{X}_{n_T} where the j^{th} candidate has coordinates

$$\tilde{x}_j = \bar{T}_j = \frac{1}{d+1} \sum_{i=1}^{d+1} T_j[i, \cdot] \quad \text{or equivalently} \quad \tilde{x}_{jk} = \frac{1}{d+1} \sum_{i=1}^{d+1} T_j[i, k]$$

for $k = 1, \dots, d$. The left expression is vectorized over the second, column dimension of T_j as is common in R and other statistical programming languages. The second is explicit about coordinates $\tilde{x}_j^\top = (\tilde{x}_{j1}, \dots, \tilde{x}_{jd})$. All of this is overkill to the verbal explanation: the j^{th} candidate is the average of the vectors describing the j^{th} triangle, so it is located in the middle of the triangle. See the red dots in Figure 2. These locations will almost certainly not be the maximal point of $\sigma_n(x)$ in the vicinity of T_j , but they will be close because \tilde{x}_j is far from T_j while being restricted to its interior. We refer to these \mathcal{X}_{n_T} as “interior” candidates.

In 2d, Euler’s formula gives that $n_T = 2n - 2 - h(X_n)$ where $h(X_n)$ is the number of elements of X_n on its convex hull. In the left panel of Figure 2, $n = 14$ and $h(X_n) = 4$ so $n_T = 22$. In the right panel, $n = 10$ and $h(X_n) = 6$ so $n_T = 12$. When $d \geq 3$, the number of faces of the tetrahedra can grow as $n^{\lceil d/2 \rceil}$ depending on the nature of X_n . Figure 3 provides an empirical view of the number of candidates for varying d and n where X_n is distributed uniformly at random in $\mathcal{B} = [0, 1]^d$. For now, focus on the dashed lines which are $\log_{10} n_T$. Notice that when n is small, n_T decreases as d increases. Perhaps more importantly, for fixed d , n_T steadily increases with n . In our BO context this is a good thing, because so too does the modality of acquisition criterion. With nonparametric surrogates like GPs, the complexity of the response surface can increase with training data size n . The fidelity of our search for the next acquisition must mimic this complexity, an innate characteristic of (internal) tricands. Figure 4, described later in Section 2.3, shows how this works after many iterations of BO, where acquisition is focused on promising EI values.

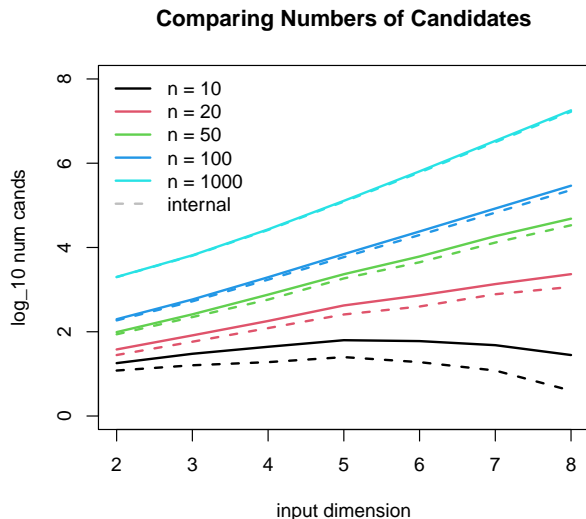


Figure 3: Numbers of candidates based on input dimension d and design size n .

2.2 Fringe candidates

Having candidates \mathcal{X}_{n_T} only in the interior of the convex hull could limit exploration if the complement of the volume of the hull and \mathcal{B} is large. It could limit exploitation if the solution is on/near the boundary of \mathcal{B} . One remedy is to force X_n to contain boundary points, such as the corners of the input space, as shown in the left panel of Figure 2. This is not a bad approach in low dimension (e.g., in 2d where there are only four corners), but could be prohibitive in higher dimension. Later in Section 3 we consider a $d = 6$ example, having 64 corners in $\mathcal{B} = [0, 1]^6$, which would blow our entire budget ($n_{\text{end}} = 50$) of runs.

We instead prefer the alternative view in the right panel of the figure, where dashed arrows represent what we refer to as “fringe” candidates. There is one of these for each facet (edge in 2d) of the convex hull, placed in the middle of the facet and extending half way to the boundary of $\mathcal{B} = [0, 1]^d$ in the direction perpendicular to that facet. Convex hull libraries like `Qhull` furnish both ingredients: $d \times d$ facets F_j and normal d -vectors \vec{v}_j for $j = 1, \dots, n_F$. Using these quantities, let $\bar{F}_j = \frac{1}{d} \sum_{i=1}^d F_j[j, i]$ denote the coordinates of the middle of facet j . Then, the j^{th} fringe candidate in \mathcal{X}_{n_F} is

$$\vec{x}_j = \bar{F}_j + \frac{\alpha_j \vec{v}_j}{2} \quad \text{where} \quad \alpha_j = \min \{ \mathbb{1}_{\{\vec{v}_j > 0\}} - \bar{F}_j \vec{v}_j \}. \quad (3)$$

Above, the min is picking out the nearest boundary to \bar{F}_j . Division by two mirrors the bisection search analogy for interior candidates. This could be a tuning parameter as we discuss further in Section 5. A non-unit rectangular \mathcal{B} is doable, but would result in a messier Eq. (3). More general \mathcal{B} may present challenges.

Fringe candidates naturally combine with internal ones to form a complete set: $\mathcal{X}_N = [\mathcal{X}_{n_T}; \mathcal{X}_{n_F}]$, stacked row-wise to form an $N \times d$ matrix with $N = n_T + n_F$. The number of fringe candidates n_F is generally small compared to n_T . This is shown empirically in Figure

3, where N is indicated by the solid line, and n_T by the dashed one. As n increases, the gap between N and n_T , indicating n_F , narrows until it is not visible on the log scale.

2.3 Random sub-sampling

Having the number of candidates N grow with the training design n may not suit all applications. Entertaining $N \approx 10\text{K}$ candidates when $n = 100$ and $d = 6$, referring to Figure 3, is cumbersome and potentially overkill. User control on fidelity-vs.-effort is key. One method to limit N is random sub-sampling: simply calculate the full \mathcal{X}_N based on X_n and downsample, uniformly at random, a subset of size $N_{\text{sub}} < N$. This is a fine idea, but in the BO context we prefer slightly more structure. Since our triangulation strategy was designed to focus on exploration (finding locally high $\sigma_n(x)$) via midway candidates, we find it advantageous to guarantee retaining some of those candidates which are promising for exploitation (low $\mu_n(x)$), still without any explicit optimization.

One of the rows of X_n corresponds to f_n^{\min} , the best input tried so far. Call this point $x_n^{\min} = x_i$ s.t. $i = \operatorname{argmin}_{i=1,\dots,n} y_i$. Let $\mathcal{T}_n^{\min} = \{T_j : x_n^{\min} \in T_j, j = 1, \dots, n_T\}$ denote the set of triangles containing x_n^{\min} , and similarly let $\mathcal{X}_n^{\min} = \{\tilde{x}_j \in \mathcal{X}_N : T_j \in \mathcal{T}_n^{\min}\}$ denote the candidates which are associated with those triangles. Those are, in a geometric sense, adjacent to x_n^{\min} . Note that a fringe candidate may also be considered adjacent in an analogous way, however we place them in the complement $\mathcal{X}_N \setminus \mathcal{X}_n^{\min}$. Now, rather than sub-sample uniformly from the full set \mathcal{X}_N , we partition sampling from points adjacent to x_n^{\min} , i.e., from \mathcal{X}_n^{\min} , and from points farther afield in $\mathcal{X}_N \setminus \mathcal{X}_n^{\min}$. In so doing, we guarantee that our N_{sub} candidates cover potential for exploitation and exploration, respectively. We prefer a 10:90 split, with up to 10% N_{sub} coming from candidates adjacent to x_n^{\min} , fewer if $|\mathcal{X}_n^{\min}| < N_{\text{sub}}$, and likewise 90% from its complement. This 10:90 split could be upgraded to a tuning parameter, but we defer this to future work.

Figure 4 provides two examples in a style similar to Figure 2, however, this time the design X_n comes after $n = 30$ runs optimizing the Goldstein–Price function with EI under varying random initializations. Details are provided in Section 3.1. When $n = 30$ we have $N \approx 60$, with the precise value depending on $h(X_n)$. Here we consider $N_{\text{sub}} = 30$. Observe how randomly sub-sampled candidates $\mathcal{X}_{N_{\text{sub}}}$, circling the original red candidates \mathcal{X}_N in green, concentrate near the global minimum $(0.5, 0.25)$ because x_n^{\min} is in the vicinity. Other sub-sampled candidates are spread out more widely. This figure also serves to illustrate how acquisitions, and thus candidates, gravitate toward promising regions for exploitation without neglecting areas of potential exploration. A ridge of local minima may be found in the banana-shaped region traced out by a concentration of X_n and \mathcal{X}_N in both views.

2.4 Implementation and software

Our implementation, provided in Python and R in our git repository on Bitbucket

<https://bitbucket.org/gramacylab/tricands/>

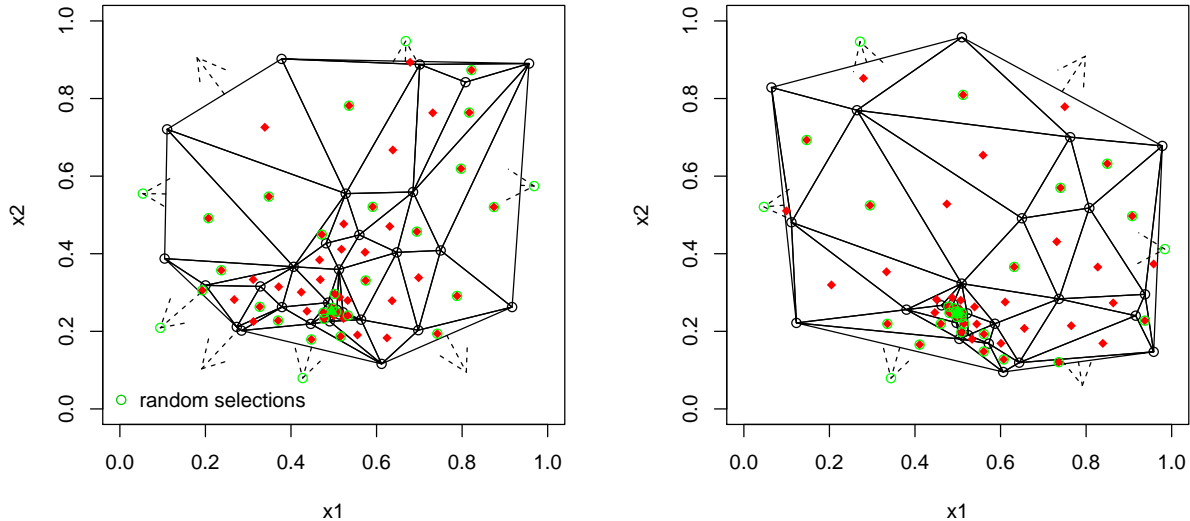


Figure 4: Illustrating interior and fringe candidates on two different random initializations of Goldstein–Price problem (Section 3.1) at $n = 30$. Legend details similar to Figure 2; randomly subsampled candidates are circled in green.

is relatively tidy. For example, `tricands.R` therein contains just 71 lines of R, 11 of which are to support optional visualizations in 2d such as those in Figures 2 and 4. The heavy lifting is done in `Qhull`. When performing Delaunay triangulations, we provide option "Q12" to work around numerical instabilities that sometimes arise. When calculating convex hulls, option "n" returns normal vectors used in calculating fringe candidates (Section 2.2).

Defaults return both fringe and internal candidates and fix a maximum candidate size of $\text{max} = N_{\text{sub}} = 100d$, but these are of course user-adjustable. In experiments coming shortly, we deliberately limit N_{sub} even further so that a fairer comparison can be made to other inner-optimization and candidate-based methods. When $N \leq N_{\text{sub}}$, all internal and fringe candidates are returned. The user may supplement these with additional $N_{\text{sub}} - N$ LHS candidates if desired. If $N_{\text{sub}} < N$, the execution flow looks for a variable `best` providing the index of x_n^{min} in X_n , making sure about 10% of tricands come from adjacent triangles. Otherwise, when `best=NULL`, tricands are sub-sampled completely at random.

3 Classical GP benchmarking

In this first of two sections on benchmarking, we focus on BO via traditional GP surrogates. We follow a homework problem in Section 7.4 of Gramacy (2020), which piggy-backs off of GP, EI and TS demonstrations earlier in the chapter. Specifically, we use the `1aGP` package for R (Gramacy, 2016; Gramacy and Sun, 2018) to fit GP surrogates with separable/automatic-relevance determination lengthscales in a Gaussian kernel using derivative-based MLE. We consider three methods of solving EI acquisitions: an inner-optimization of the criterion via L-BFGS-B with 5-multi-starts, LHS candidates via `lhs` (Carnell, 2018), and our own

tricands. For TS acquisitions, we similarly employ both LHS candidates and tricands. For non-surrogate optimization comparisons, we provide L-BFGS-B and Nelder–Mead (Nelder and Mead, 1965) local optimizers via `optim` in R. These under-perform the BO alternatives, but nevertheless serve as an important benchmark.

We showcase two examples, which, along with those in Section 4, are described in more detail on the pages of the Virtual Library for Simulation Experiments (VLSE; Surjanovic and Bingham, 2013). Throughout, we code inputs to $[0, 1]^d$. In each case we perform a Monte Carlo experiment, restarted 100 times, where each GP-based comparator is initialized with the same starting design of size $n_0 = 12$. This design is taken uniformly at random following the advice of Zhang et al. (2021) who caution that small space-filling initial designs can spark pathological behavior in BO. We track “best observed value” (BOV) f_n^{\min} as a measure of progress which is summarized by median over $n = 1, \dots, n_{\text{end}}$ and by boxplots for particular n along the way. We also control and keep track of the number of evaluations of the acquisition criteria for each method. Other problem-specific details are provided as needed.

To foreshadow somewhat, these two examples are chosen because they work well with a traditional GP/EI setup. In particular, the deployment of standard, library-based GPs means that criteria like EI can be optimized with library methods. This is in contrast to the examples coming next in Section 4. Those are not well-fit by ordinary GPs because of their regime-changing behavior, and so we must entertain higher-powered alternatives with more limited support for solving for acquisitions. Reproducible code for all of the examples in Sections 3–4 is provided in our git repository.

3.1 Goldstein–Price

The Goldstein–Price function is a common, low-dimensional (2d) benchmark for BO (e.g., Picheny et al., 2012). Here we follow the VLSE specification at the link below.

<https://www.sfu.ca/~ssurjano/goldpr.html>

A total of $n_{\text{end}} = 50$ acquisitions are entertained, and all candidate-based methods (tricands and LHS) are limited to fifty candidates. This means $\max = N_{\text{sub}} = 50$ for tricands, and that fewer may potentially be used when $N < N_{\text{sub}}$. Figure 5 summarizes results in three views. In the left panel, median progress in BOV is shown over increasing budgets of evaluations, n , as if each subsequent acquisition were the last. In the middle and right panels, boxplots capture the distribution of BOV at $n = 30$ and $n = 50$, respectively. In the left panel, methods based on BFGS (inner/EI) optimization use solid lines; those based on tricands are dashed; those based on LHS candidates are dotted. (Nelder–Mead is an exception, being red-dashed.) In the boxplots, tricands use slightly thicker lines and dots so that they stand out. Text printed at the top of the right panel indicates the average number of times the criterion, EI or TS, was evaluated in solving the inner optimization sub-problem(s), cumulative over all acquisitions. In the case of BFGS-based EI (labeled “EI”), these happen within the iterations of the L-BFGS-B inner optimizer.

Beginning with medians over n in the left panel, observe that the dashed lines (those based on tricands) are uniformly superior to all other comparators. EI with tricands is slightly bet-

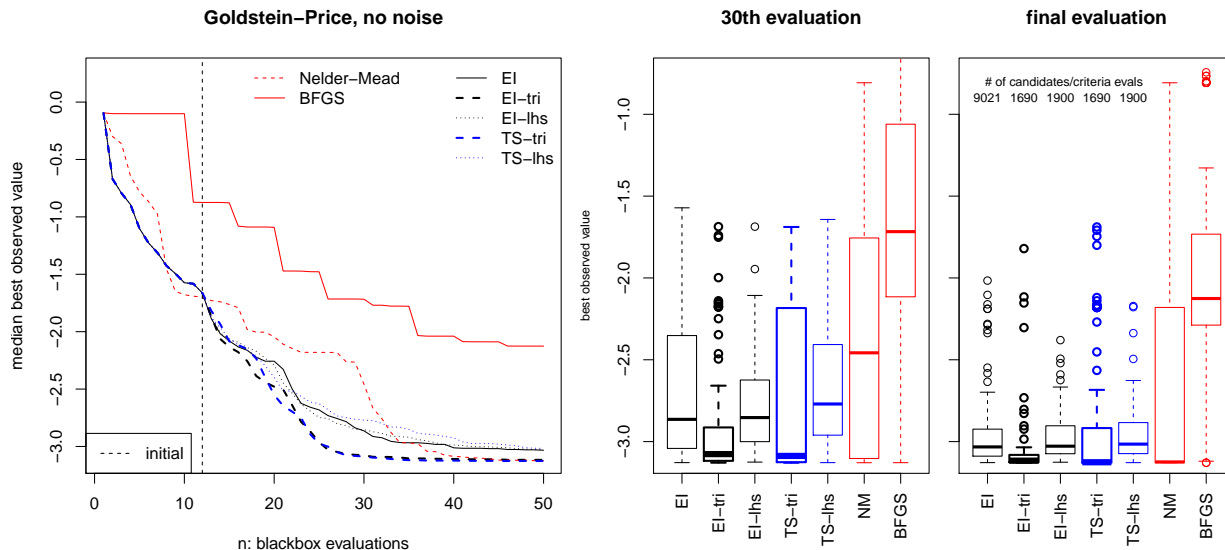


Figure 5: Goldstein-Price optimization 100 MC trials via median BOV progress (left panel) and the full distribution at 30th (middle) and final (50th, right) acquisition.

ter than TS with tricands. Only at the very end of the run does the Nelder-Mead alternative look competitive. At the 30th evaluation (middle panel) the boxplots indicate that there are some MC repetitions where the BOV based on tricands are underperforming. However, more than half of the time these are the best two (i.e., both EI and TS with tricands) of all. TS with tricands is the winner in terms of best-case performance, whereas the EI version has slightly better worst-case behavior. Neither local optimizer (red) is competitive. Finally, in the right panel we see that the story is similar, except that now EI with tricands seems to edge out its TS analog. Although median performance for Nelder-Mead is competitive, more than half of the time its BOV at $n_{\text{end}} = 50$ is among the two worst in the experiment. All of the methods have some relatively high outlying BOV values, although we caution that the scale of the y -axis of these plots is different than that for the left panel, showing only median progress. As always with BO, you can get unlucky with initialization, or conversely lucky with other random aspects of a search. This explains many of the outlying dots in the boxplots for all BO comparators, none of which is consistently under-performing. All of them find the answer with low variability using a slightly larger n_{end} , but extending out in that direction makes for a less interesting comparison.

Perhaps the most striking result from the figure is that tricands-based EI outperforms its inner-BFGS analog despite a factor of five fewer evaluations of the EI criterion (about 9000 compared to 1700). A more aggressive, derivative-based search misutilizes computational resources. Finding a precise solution – ultimately furnishing a maximal local value in an inferior domain of a attraction – may come at the expense of finding an accurate approximation nearby a global solution. The same is true, but to a lesser extent, when comparing TS variations (a difference of about 100, or about 5%).

3.2 Hartmann 6

Next we consider the six-dimensional Hartmann function. Again, see (Picheny et al., 2012) for more on this benchmark, or the description on VLSE.

<https://www.sfu.ca/~ssurjano/hart6.html>

Our experimental setup is identical to the one above except we entertain up to 600 candidates (i.e., the default tricands setting of $N_{\text{sub}} = 100d$). Figure 6 summarizes the results. Even with this high N_{sub} , the evaluations of the inner optimization criterion (top of right panel) are many fewer than those of BFGS-based EI, which must search more aggressively for the local optimum in such high dimension.

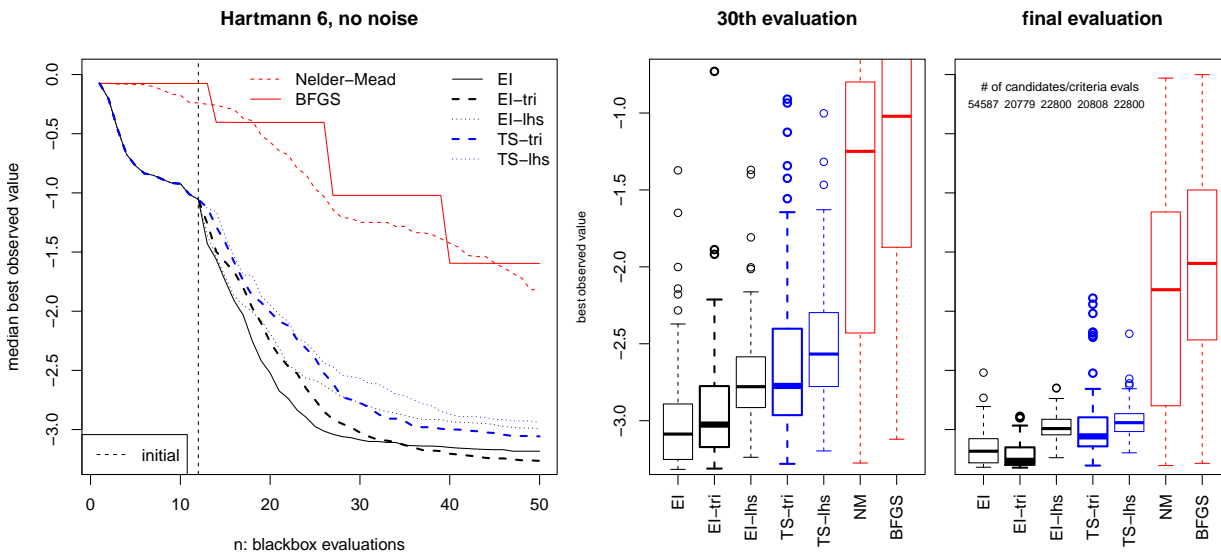


Figure 6: Analog of Figure 5 for the Hartmann 6 function.

The results of this experiment are largely similar to our earlier 2d Goldstein–Price example. Tricands-based EI yields equivalent, or better, BOV despite many fewer criteria evaluations. This is true, but to a lesser extent, with TS. It is notable that tricands come from behind in the case of EI. For the first twenty or so acquisitions, ordinary BFGS-based EI is outperforming its tricands variation. Apparently, a geometric bias towards exploration is less desirable in early acquisitions, but pays off by the end of the search. Tricands EI is the clear winner by $n_{\text{end}} = 50$.

4 Nonstationary GP benchmarking

Tricands are arguably most valuable when the inner-optimization problem cannot be solved by library-based methods, such as L-BFGS-B, even locally. This happens when the surrogate predictive surface is discontinuous, thwarting derivative-based methods, and/or when

inference requires MCMC. It is technically possible to optimize an objective based on approximate ergodic averages – derivatives of sums are sums of derivatives, after all. One approach, leveraging common random numbers, is known sample average approximation (SAA; Verweij et al., 2003). However, implementation in practice is cumbersome and is not supported by any of the MCMC-based surrogate modeling libraries that we are aware of. Candidate-based acquisition is the *modus operandi* in this context.

We have two specific examples in mind, both of which make for popular surrogate modeling choices when the response surface exhibits nonstationarity, meaning that the input–output dynamics evolve over the input space. When those dynamics are not well-modeled by purely relative-distance-based structures, which are the default in GP surrogate modeling, one needs a more elaborate model. A treed Gaussian process (TGP; Gramacy and Lee, 2008) uses axis-aligned partitioning with GPs. This divide-and-conquer approach excels when dynamics change abruptly across individual inputs creating distinct regimes. MCMC is used to average over the location of probable partition boundaries, as well as other parameters describing the process. We use the R package `tgp` on CRAN (Gramacy, 2007), following Section 4 of Gramacy and Taddy (2010) for candidate-based EI acquisition.

The other is a deep Gaussian process (DGP; Damianou and Lawrence, 2013). DGPs warp inputs to accommodate a more subtle evolution of dynamics in the input space compared to the abrupt regime changes of TGP. Although variational inference is popular for DGPs (Salimbeni and Deisenroth, 2017), Sauer et al. argue that in active learning contexts, such as BO, full posterior approximation (say by MCMC) leads to better uncertainty quantification, and thus provides better acquisitions for expensive blackbox evaluation. Here we use the R package `deepgp` on CRAN (Sauer, 2021) which supports EI evaluation on candidates.

Unfortunately, neither `tgp` nor `deepgp` easily facilitate TS acquisition for BO. Taking a single draw from the posterior predictive distribution at a pre-defined set of candidates, but at the same time averaging over the posterior distribution of all unknowns, would require the use of common random numbers (like SAA for EI above). Neither package allows the user any control over the random deviates deployed in sampling. We therefore do not include TS in our comparisons here. However, the `tgp` package can return the maximum *a posteriori* (MAP) sample which can be used as the basis of a local BFGS scheme (Gramacy and Taddy, 2010, Section 4). Following a candidate search with a derivative-based one initialized at the best candidate is extra work, but often pays off. Here we show that `tracands` provides better candidates for both pure candidate search and this hybrid two-stage scheme.

4.1 Abrupt: Gramacy & Lee/Michaelwicz

The Gramacy & Lee (G&L) function, first introduced with TGP as a prototypical test case, benefits from a model supporting hard breaks even though its dynamics evolve smoothly.

<https://www.sfu.ca/~ssurjano/grlee08.html>

Although low dimensional, the input domain (which we code to $[0, 1]^2$) is set up so that three quarters of the input space are essentially flat. In the “interesting quadrant” a local maximum is twinned with a (global) minimum, disguising it from the rest of the input space

in some perspectives. Moreover, the domain of attraction of that global minimum covers only about 10% of the input space. It is easily missed by random initial designs and candidate sets, which makes this a challenging BO benchmark. TGP is able to isolate the interesting quadrant with just two axis aligned partitions and, in so doing, recognize that sampling effort should be concentrated there.

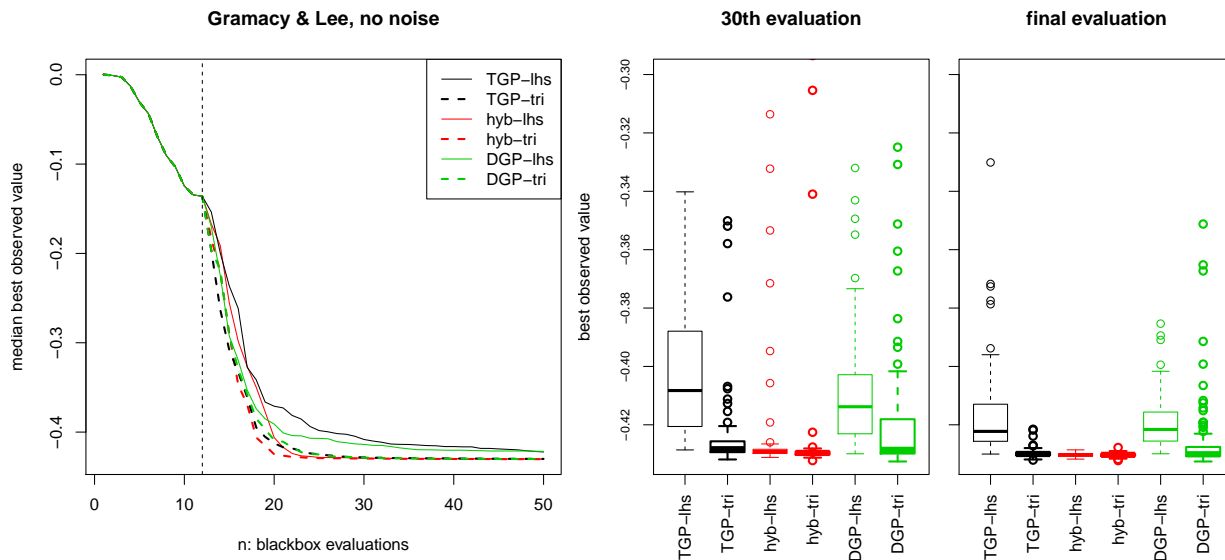


Figure 7: Gramacy & Lee function with MCMC-based comparators.

Figure 7 shows results in the same three views as earlier. The number of candidates is limited to twenty, otherwise the setup is unchanged. First ignore the red lines and boxplots (those labeled “hyb-”) and focus on the black (TGP) and green (DGP). Notice that in both cases the tricands-based comparators, dashed and/or bolded, outperform their LHS-based analogues. In terms of medians over n (left panel), that dominance is uniform. In terms of boxplots, the disparity is stark with the exception of a few outlying DGP-based BOV values with tricands. TGP seems to edge out DGP (with tricands) which we attribute to the abrupt change between interesting quadrant and the rest of the input space. Now focus on the red “hyb-” results. These are the ones where TGP candidate-based search is finished with a derivative-based EI calculation on the MAP model. Although it’s hard to tell the difference between the LHS and tricands based results after $n = 22$ in the left panel, or for either $n = 30$ or 50 in the other panels, we can report that tricands BOV value was lower in 88/100 MC reps in the former (middle panel) and 97/100 in the latter (right panel). This is a clear win for tricands.

As a second example of abruptly changing regimes, consider the Michaelwicz function.

<https://www.sfu.ca/~ssurjano/michal.html>

Like G&L, the surface has large flat areas, but it also has a continuum of ridges of local minima which intersect to create deeper valleys of local minima, and ultimately one global

minimum where the deepest of those ridges intersect. A nice feature of the Michaelwicz function is that it is defined in arbitrary input dimension. Here we use it in 4d, which makes for a very challenging surface to model and optimize. To cope, we take the search out to $n_{\text{end}} = 75$ and allow up to two hundred candidates per acquisition. Otherwise the setup is similar to earlier examples. Figure 8 shows the results, which are largely similar to G&L,

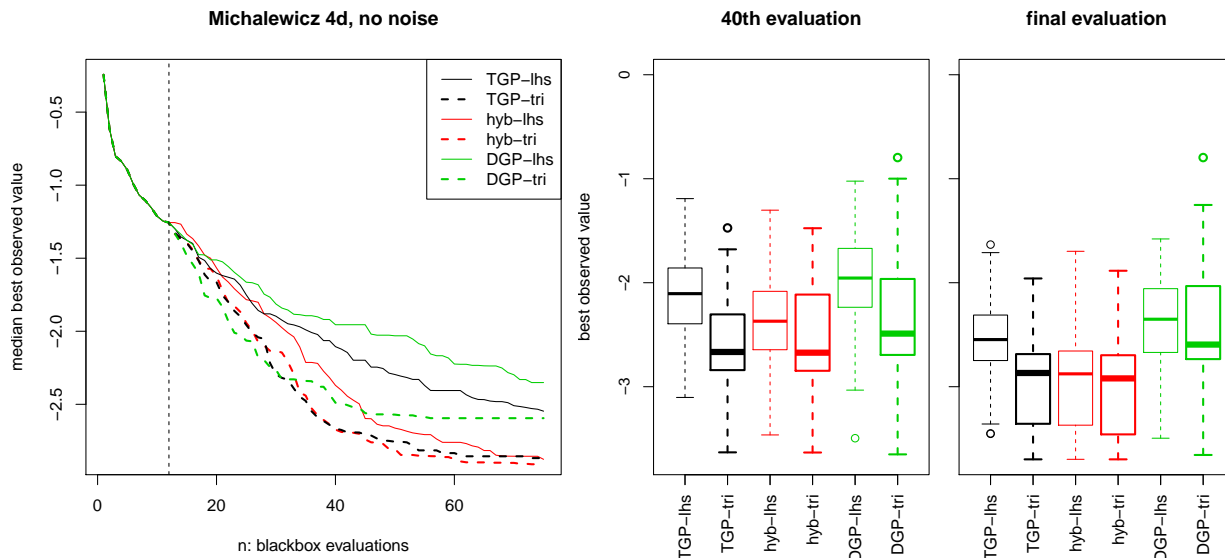


Figure 8: Michaelwicz function in 4d with MCMC-based comparators.

except revealing of these additional challenges. Tricands uniformly dominate LHS via median BOV. Although noise is high across all boxplots, reflecting variability in solution quality over random re-initialization, the patterns are clear in a pairwise analysis. For example, the red boxplots in the right panel look similar but, at the 75th evaluation, 75/100 tricands-based BOVs were below their LHS counterpart. As in the G&L example, TGP seems to outperform DGP. Abrupt regime changes are at odds with the DGP’s smooth warping of the input space.

4.2 Smooth: Levy

The Levy function is similar to Michaelwicz in that it is defined in arbitrary dimension and has many local minima but only one global solution, yet it is otherwise better behaved.

<https://www.sfu.ca/~ssurjano/levy.html>

There are no flat regions. It is ruffled with many peaks and valleys, but has no sub-manifolds of constant value that could fool an optimizer. Here we consider $d = 5$ for variety; see Figure 9. Commensurate with other similarly sized examples, we consider up to two hundred candidates and $n_{\text{end}} = 75$.

Both candidate DGP variations outperform their TGP counterparts. Slowly/smoothly varying dynamics favor warping inputs as opposed to hard partitioning. This is evident in

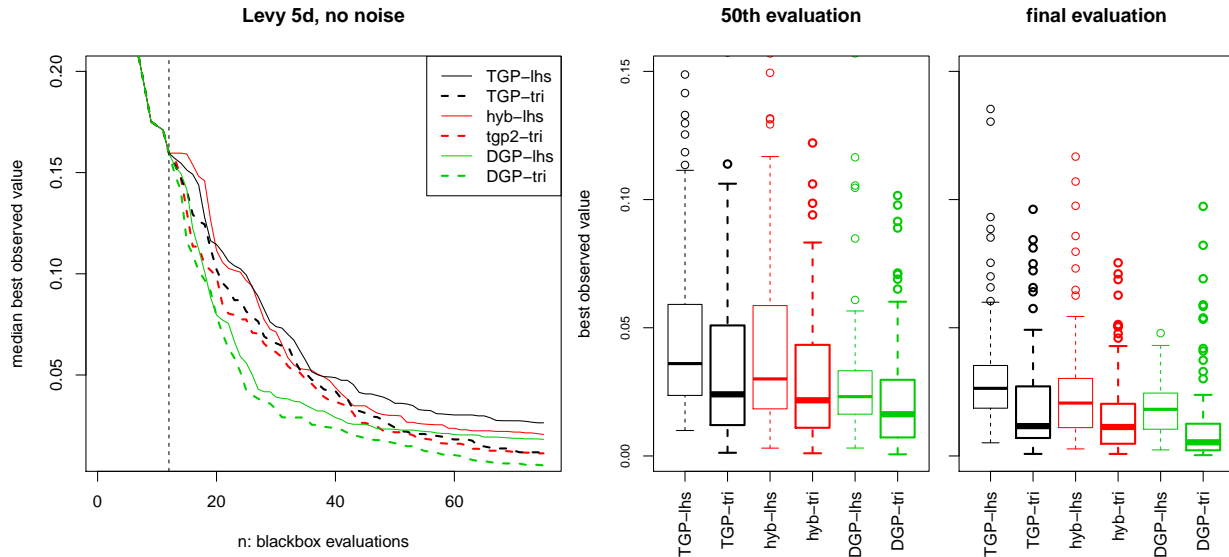


Figure 9: Levy function in 5d with MCMC-based comparators.

both median and full distribution (boxplot) views. In the median view (left panel), notice that the dashed lines are uniformly under the solid ones of the same color. Tricands are providing better median performance over all n . Although the preeminence of tricands is apparent visually, we report that tricands provided better BOV in 81/100 MC restarts among the best (DGP) comparators. When tricands are involved, the hybrid candidate/BFGS option is not discernably better than the pure candidate alternative in terms of median progress or final distribution of BOV. Its thrifty geometric criterion is an adequate substitute for, if not substantially superior to, aggressive acquisition criterion optimization.

5 Discussion

We offer a novel take on space-filling candidates for acquisition in Bayesian optimization (BO). Rather than filling the entire space, our Delaunay triangulation-based candidates (“tricands”) fill the spaces in-between previous acquisitions. This is motivated by an analogy to bisection search, but also by the nature of Gaussian process (GP) predictive surfaces which often serve as surrogates in BO. GP surrogates have organically inflated uncertainty between training data sites, which makes those spots attractive for BO acquisition. This notion is extended to the space between the convex hull of existing training data and the boundary \mathcal{B} of the study region. In an array of benchmark exercises we have demonstrated that tricands lead to superior performance in BO compared to both higher-powered derivative-based acquisition schemes and simpler space-filling candidate sets. The main advantage of tricands is that they mimic the behavior of those higher-powered searches – usually out-performing them – with the implementation simplicity of a candidate scheme. That simplicity means that tricands may be deployed where the higher-powered alternatives cannot, such as when the surrogate

is not continuous or requires Monte Carlo inference.

When reflecting on tricands’ value, it is important to remember some stylized facts about BO. One is that the theory (under stringent regularity conditions) guarantees convergence to the global minimum “eventually,” in the sense that with enough samples you’ll explore everywhere (e.g., Bull, 2011). That’s not much help in practice, because exploring everywhere isn’t practical. Another is that EI and TS are greedy; their scope is the next acquisition. Contemplating a remaining budget and entertaining optimal decisions through that lens can be caricatured as a herculean effort with marginal gains (Gonzalez et al., 2016; Frazier et al., 2008; Lam et al., 2016; Gramacy and Lee, 2011). These are not bad ideas, but they haven’t moved the needle on the *modus operandi* because they’ve not been incorporated into accessible libraries, and are too involved for bespoke implementation.

Both theory and aggressively scoped acquisition can lose sight of the real goal. What’s important in BO, and active learning in general, is creating a virtuous cycle between data acquisition and learning. Anyone who has tried knows that there is a fine line between vicious and virtuous when it comes to implementation details, despite the best of intentions and theoretical “guarantees”. EI and TS are simple to implement because GP libraries are in abundance, code evaluating criteria is a few lines long, and there are many examples to cut-and-paste from. Barriers to application are low, but it’s easy to get carried away to disappointment. This is what makes tricands attractive. It is plug-and-play and motivated by simple principles: the solution is in-between your current runs, so look there.

That’s not to say that tricands are a panacea. Some of our boxplots indicated that improvements over alternatives on best-observed-value (BOV) in 90/100 MC repetitions may have come at the expense of the worst case performance of the remaining 10%. This may have simply been bad luck. But if not, the deterministic nature of tricands may be to blame: not enough opportunity to be surprised. As mentioned in the main body of the paper, one can always augment tricands with LHS or other space-filling candidates. This could be especially beneficial when N , the number of tricands for a given n , is lower than the desired budget of candidates. Entertaining tuning parameters for some of our hard-coded settings, like the distance between fringe candidates and the boundary (Section 2.2), could help. That distance could even be chosen at random. We could likewise randomly choose a location for interior candidates (Section 2.1), within each triangle, rather than taking the center. When randomly downsampling (Section 2.3), we could guarantee a certain proportion of fringe candidates like we did for ones adjacent to f_n^{\min} .

Although the important subroutines of Delaunay triangulation and convex hulls are off-loaded to libraries, they can (at times) be computationally demanding. When n is large and d is modest, calculating N locations in the thousands (see Figure 3) could be cumbersome. Of course, the whole goal of BO is to limit n . In our experiments with $n \leq 75$, all of our triangulation/hull calculations took fractions of a second. But with big n they can take minutes, and that could be prohibitive. However, after each acquisition the number of new sites only increases by one ($n \rightarrow n + 1$), and thus affects only a small, local part of the triangulation/hull. The `Qhull` library does not support this, but there are incremental algorithms for triangle/hull augmentation which are very fast relative to starting from scratch.

For more details, see Su and Drysdale (1997).

Such a strategy might be valuable in higher dimensional BO settings. Continuous optimization theory tells us that gradient-based methods have local convergence rates independent of dimension, which has made L-BFGS-B and similar optimizers the tool of choice in solving for acquisitions. This, together with the exponential growth of input space volume, might at first blush suggest that tricands’ performance is limited to low dimension. However, in practice, the highly nonconvex nature of the acquisition surface significantly cheapens the theoretical results associated with gradient-based optimization. Indeed, recent work has achieved state-of-the-art performance in high d using candidate sets focused within a certain region of the input space (Eriksson et al., 2019; Daulton et al., 2021), though still built on traditional space-filling points such as LHS. It would be interesting to see whether replacing these space-filling points with tricands would be as beneficial in that setting as we have found it to be in low d . Furthermore, a popular approach in scaling BO to high dimension is to reduce the input space by screening input variables or finding linear or nonlinear embedding spaces, rendering the problem a low dimensional one (see Binois and Wycoff (2021) for an overview). The aim of such an approach is in part to make solving the acquisition problem easier, and there’s no reason to believe this wouldn’t extend to tricands.

We considered only deterministic blackbox objectives f in this paper. Surrogate modeling via GPs is easily extended to handle noisy data. If the noise level is varying throughout the input space (i.e., heteroskedasticity), that process could be rather more involved (Binois et al., 2018). Surrogate modeling and active learning for stochastic simulation is still very much on the frontier of the computer experiments landscape (Baker et al., 2020). In such settings, the acquisition space must be extended to include the possibility of obtaining a replicate run, duplicating one of the n existing design elements (Binois et al., 2019). Replication can be advantageous in separating signal from noise in generic active learning tasks, and specifically in the context of BO (Binois and Gramacy, 2021, Section 4.2). Rather than entertaining a hybrid search between a continuum of novel locations, and a discrete set of replicate sites, tricands could be leveraged to make the entire set of candidates discrete, vastly simplifying the inner optimization search.

Batch acquisition, acquiring several new sites at once, is a common paradigm in some settings. Ideas with modified EI go back at least to Ginsbourger et al. (2007) with several following thereafter (e.g., Taddy et al., 2009; Chevalier and Ginsbourger, 2013). One, more recent approach involves penalizing regions of the input space near earlier acquisitions in the batch (González et al., 2016). This spirit could be ported to a tricands setting: simply rule out any candidates which are in triangles adjacent to those acquired earlier in the batch.

Finally, although we have emphasized BO, other active learning criteria could benefit from candidates well-spaced relative to the current design. Perhaps the most common is design targeting reduced integrated mean-squared prediction error (IMSPE, e.g., Leatherman et al., 2017; Binois et al., 2019; Zhang et al., 2020a). High input variance locations, such as between design sites, are natural candidates for reducing IMSPE. Another recently popular active learning topic in computer experiments is contour/level set finding (Ranjan et al., 2008; Bect et al., 2012; Chevalier et al., 2014; Marques et al., 2018; Azzimonti et al., 2020; Cole et al.,

2021). Many of the criteria suggested in these works involve predictive entropy from a GP surrogate, which is famously myopic: entropy (defined via a classification above and below a level set) tends to be higher near training data already near partition boundaries, leading to a clumping of acquisitions unless explicit measures are taken to spread out candidates, or to otherwise deter a numerical inner-optimizer. Tricands could offer a geometric spread of future acquisitions away from existing training data locations.

Acknowledgments

We are grateful for funding from DOE LAB 17-1697 via subaward from Argonne National Laboratory for SciDAC/DOE Office of Science ASCR and High Energy Physics.

References

- Azzimonti, D., Ginsbourger, D., Chevalier, C., Bect, J., and Richet, Y. (2020). “Adaptive design of experiments for conservative estimation of excursion sets.” *Technometrics*, 1–14.
- Baker, E., Barbillon, P., Fadikar, A., Gramacy, R. B., Herbei, R., Higdon, D., Huang, J., Johnson, L. R., Ma, P., Mondal, A., et al. (2020). “Analyzing stochastic computer models: A review with opportunities.” *arXiv preprint arXiv:2002.01321*.
- Barber, C. B., Dobkin, D. P., and Huhdanpaa, H. (1996). “The Quickhull Algorithm for Convex Hulls.” *ACM Trans. Math. Softw.*, 22, 4, 469–483.
- Bect, J., Ginsbourger, D., Li, L., Picheny, V., and Vazquez, E. (2012). “Sequential design of computer experiments for the estimation of a probability of failure.” *Statistics and Computing*, 22, 3, 773–793.
- Binois, M., Gramacy, R., and Ludkovski, M. (2018). “Practical heteroscedastic Gaussian process modeling for large simulation experiments.” *Journal of Computational and Graphical Statistics*, 27, 4, 808–821.
- Binois, M. and Gramacy, R. B. (2021). “hetGP: Heteroskedastic Gaussian Process Modeling and Sequential Design in R.” *Journal of Statistical Software*, 98, 13, 1–44.
- Binois, M., Huang, J., Gramacy, R., and Ludkovski, M. (2019). “Replication or exploration? Sequential design for stochastic simulation experiments.” *Technometrics*, 27, 4, 808–821.
- Binois, M. and Wycoff, N. (2021). “A survey on high-dimensional Gaussian process modeling with application to Bayesian optimization.”
- Bull, A. (2011). “Convergence rates of efficient global optimization algorithms.” *Journal of Machine Learning Research*, 12, Oct, 2879–2904.
- Burden, R. and Faires, J. (1985). *Numerical Analysis*. PWS Publishers.

- Byrd, R., Lu, P., Nocedal, J., and Zhu, C. (2003). “A Limited Memory Algorithm for Bound Constrained Optimization.” *SIAM Journal on Scientific Computing*, 16.
- Carnell, R. (2018). *lhs: Latin Hypercube Samples*. R package version 0.16.
- Chevalier, C., Bect, J., Ginsbourger, D., Vazquez, E., Picheny, V., and Richet, Y. (2014). “Fast parallel kriging-based stepwise uncertainty reduction with application to the identification of an excursion set.” *Technometrics*, 56, 4, 455–465.
- Chevalier, C. and Ginsbourger, D. (2013). “Fast computation of the multi-points expected improvement with applications in batch selection.” In *International Conference on Learning and Intelligent Optimization*, 59–69. Springer.
- Cole, D. A., Gramacy, R. B., Warner, J. E., Bomarito, G. F., Leser, P. E., and Leser, W. P. (2021). “Entropy-based adaptive design for contour finding and estimating reliability.” *arXiv preprint arXiv:2105.11357*.
- Damianou, A. and Lawrence, N. D. (2013). “Deep gaussian processes.” In *Artificial intelligence and statistics*, 207–215. PMLR.
- Daulton, S., Eriksson, D., Balandat, M., and Bakshy, E. (2021). “Multi-Objective Bayesian Optimization over High-Dimensional Search Spaces.”
- Eriksson, D., Pearce, M., Gardner, J., Turner, R. D., and Poloczek, M. (2019). “Scalable Global Optimization via Local Bayesian Optimization.” In *Advances in Neural Information Processing Systems*, 5497–5508.
- Feurer, M., Letham, B., Hutter, F., and Bakshy, E. (2018). “Practical Transfer Learning for Bayesian Optimization.” *arXiv preprint arXiv:1802.02219*.
- Frazier, P. I., Powell, W. B., and Dayanik, S. (2008). “A knowledge-gradient policy for sequential information collection.” *SIAM Journal on Control and Optimization*, 47, 5, 2410–2439.
- Garnett, R. (2022). *Bayesian Optimization*. Cambridge University Press. In preparation.
- Ginsbourger, D., Le Riche, R., and Carraro, L. (2007). “A multi-points criterion for deterministic parallel global optimization based on kriging.” In *NCP07*.
- González, J., Dai, Z., Hennig, P., and Lawrence, N. (2016). “Batch Bayesian optimization via local penalization.” In *Artificial intelligence and statistics*, 648–657. PMLR.
- Gonzalez, J., Osborne, M., and Lawrence, N. (2016). “GLASSES: Relieving the myopia of Bayesian optimisation.” In *Proceedings of the 19th International Conference on Artificial Intelligence and Statistics*, 790–799.

- Gramacy, R. (2007). “**tgp**: an R Package for Bayesian Nonstationary, Semiparametric Non-linear Regression and Design by Treed Gaussian Process Models.” *Journal of Statistical Software*, 19, 9, 6.
- (2016). “**1aGP**: large-scale spatial modeling via local approximate Gaussian processes in R.” *Journal of Statistical Software*, 72, 1, 1–46.
- Gramacy, R. and Lee, H. (2008). “Bayesian treed Gaussian process models with an application to computer modeling.” *Journal of the American Statistical Association*, 103, 483, 1119–1130.
- Gramacy, R. and Lee, H. K. (2011). “Optimization under unknown constraints.” In *Bayesian Statistics*, vol. 9. Oxford University Press.
- Gramacy, R. and Sun, F. (2018). *1aGP: Local Approximate Gaussian Process Regression*. R package version 1.5-3.
- Gramacy, R. and Taddy, M. (2010). “Categorical inputs, sensitivity analysis, optimization and importance tempering with **tgp** version 2, an R package for treed Gaussian process models.” *Journal of Statistical Software*, 33, 6, 1–48.
- Gramacy, R. B. (2020). *Surrogates: Gaussian Process Modeling, Design and Optimization for the Applied Sciences*. Boca Raton, Florida: Chapman Hall/CRC. <http://bobby.gramacy.com/surrogates/>.
- Habel, K., Grasman, R., Gramacy, R. B., Mozharovskiy, P., and Sterratt, D. C. (2019). *geometry: Mesh Generation and Surface Tessellation*. R package version 0.4.5.
- Jones, D. R., Schonlau, M., and Welch, W. J. (1998). “Efficient global optimization of expensive black-box functions.” *Journal of Global optimization*, 13, 4, 455–492.
- Kim, H., Mallick, B., and Holmes, C. (2005). “Analyzing nonstationary spatial data using piecewise Gaussian processes.” *Journal of the American Statistical Association*, 100, 470, 653–668.
- Lam, R., Willcox, K., and Wolpert, D. H. (2016). “Bayesian optimization with a finite budget: An approximate dynamic programming approach.” *Advances in Neural Information Processing Systems*, 29, 883–891.
- Leatherman, E., Santner, T., and Dean, A. (2017). “Computer experiment designs for accurate prediction.” *Statistics and Computing*, 1–13.
- Letham, B. and Bakshy, E. (2019). “Bayesian Optimization for Policy Search via Online-Offline Experimentation.” *J. Mach. Learn. Res.*, 20, 145–1.
- Marques, A., Lam, R., and Willcox, K. (2018). “Contour location via entropy reduction leveraging multiple information sources.” In *Advances in Neural Information Processing Systems*, 5217–5227.

- Mckay, D., Beckman, R., and Conover, W. (1979). “A Comparison of Three Methods for Selecting Vales of Input Variables in the Analysis of Output From a Computer Code.” *Technometrics*, 21, 239–245.
- Močkus, J. (1975). “On Bayesian methods for seeking the extremum.” In *Optimization techniques IFIP technical conference*, 400–404. Springer.
- Nelder, J. and Mead, R. (1965). “A simplex method for function minimization.” *The Computer Journal*, 7, 4, 308–313.
- Picheny, V., Wagner, T., and Ginsbourger, D. (2012). “A benchmark of kriging-based infill criteria for noisy optimization.” *Structural and Multidisciplinary Optimization*, 1–20.
- Pourmohamad, T. and Lee, H. K. (2021). *Bayesian Optimization with Application to Computer Experiments*. New York, NY: Springer.
- Ranjan, P., Bingham, D., and Michailidis, G. (2008). “Sequential experiment design for contour estimation from complex computer codes.” *Technometrics*, 50, 4, 527–541.
- Rushdi, A., Swiler, L., Phipps, E., D’Elia, M., and Ebeida, M. (2017). “VPS: Voronoi piecewise surrogate models for high-dimensional data fitting.” *International Journal for Uncertainty Quantification*, 7, 1.
- Salimbeni, H. and Deisenroth, M. (2017). “Doubly stochastic variational inference for deep Gaussian processes.” *arXiv preprint arXiv:1705.08933*.
- Sauer, A. (2021). **deepgp**: *Sequential Design for Deep Gaussian Processes using MCMC*. R package version 0.3.0.
- Sauer, A., Gramacy, R. B., and Higdon, D. (2020). “Active Learning for Deep Gaussian Process Surrogates.” *arXiv preprint arXiv:2012.08015*.
- Su, P. and Drysdale, R. L. S. (1997). “A comparison of sequential Delaunay triangulation algorithms.” *Computational Geometry*, 7, 5-6, 361–385.
- Surjanovic, S. and Bingham, D. (2013). “Virtual library of simulation experiments: test functions and datasets.” <http://www.sfu.ca/~ssurjano>.
- Taddy, M., Lee, H., Gray, G., and Griffin, J. (2009). “Bayesian guided pattern search for robust local optimization.” *Technometrics*, 51, 4, 389–401.
- Thompson, W. R. (1933). “On the likelihood that one unknown probability exceeds another in view of the evidence of two samples.” *Biometrika*, 25, 3/4, 285–294.
- Turner, R., Eriksson, D., McCourt, M., Kiili, J., Laaksonen, E., Xu, Z., and Guyon, I. (2021). “Bayesian optimization is superior to random search for machine learning hyperparameter tuning: Analysis of the black-box optimization challenge 2020.” *arXiv preprint arXiv:2104.10201*.

- Verweij, B., Ahmed, S., Kleywegt, A. J., Nemhauser, G., and Shapiro, A. (2003). “The sample average approximation method applied to stochastic routing problems: a computational study.” *Computational optimization and applications*, 24, 2, 289–333.
- Zhang, B., Cole, D. A., and Gramacy, R. B. (2021). “Distance-distributed design for Gaussian process surrogates.” *Technometrics*, 63, 1, 40–52.
- Zhang, B., Gramacy, R. B., Johnson, L., Rose, K. A., and Smith, E. (2020a). “Batch-sequential design and heteroskedastic surrogate modeling for delta smelt conservation.” *arXiv preprint arXiv:2010.06515*.
- Zhang, Y., Apley, D. W., and Chen, W. (2020b). “Bayesian optimization for materials design with mixed quantitative and qualitative variables.” *Scientific reports*, 10, 1, 1–13.